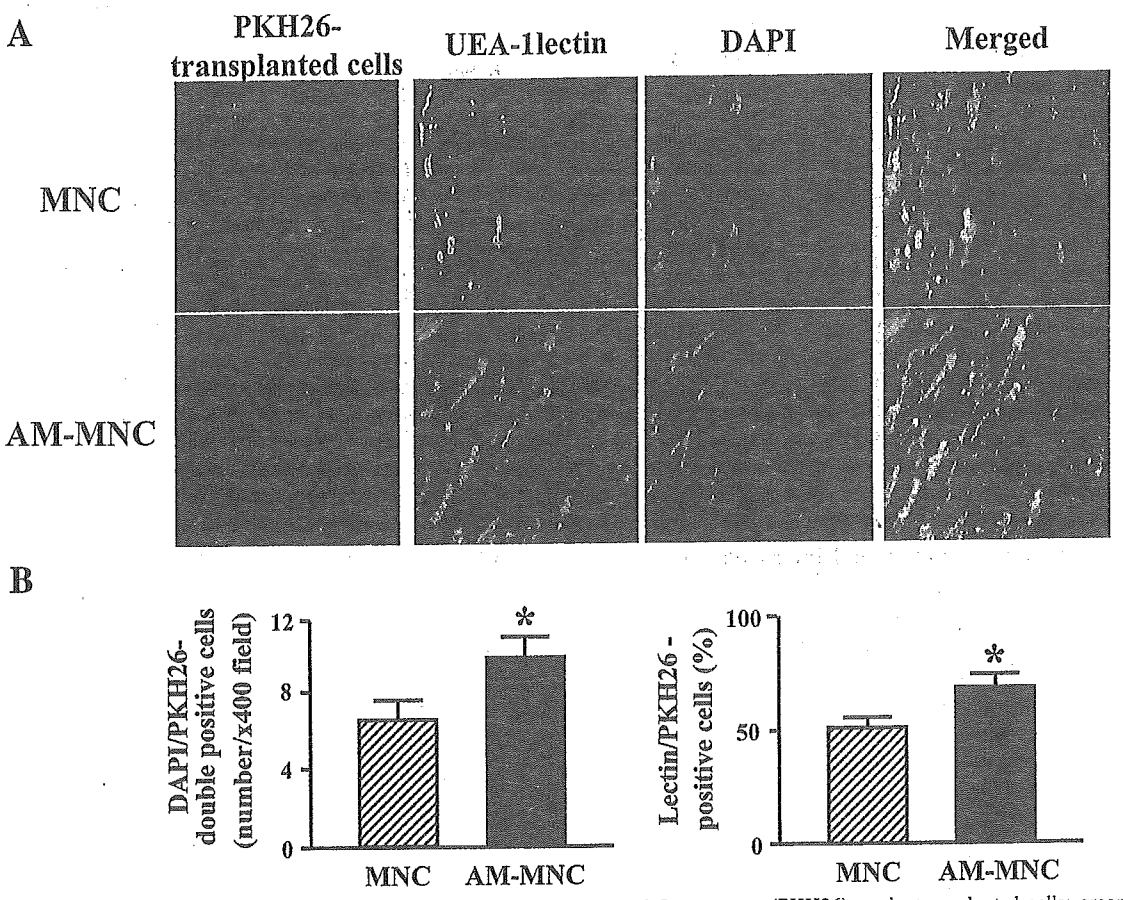

Fig. 5. *A*: representative examples of MNC differentiation into endothelial lineage. Red fluorescence (PKH26) marks transplanted cells; green fluorescence indicates ulex europaeus (UEA)-1 lectin, a marker for vascular endothelial cells. Most of the transplanted cells differentiated into endothelial cells in the AM-MNC group. Magnification, ×400. *B*: quantitative analysis of living transplanted cells and endothelial differentiation. The number of living cells after transplantation was significantly higher in the AM-MNC group than in the MNC group. The ratio of lectin-positive cells to living transplanted cells was significantly higher in the AM-MNC group than in the MNC group. Values are means ± SE. $^*P < 0.05$ vs. control. DAPI, 4′,6′-diamidino-2-phenylindole.

study (18). These findings suggest that the reduction of infarct size induced by this combination therapy may be attributable to additive cardioprotective effects of MNC and AM.

The present study showed that AM infusion significantly increased capillary density in ischemic myocardium. Furthermore, AM infusion plus MNC transplantation demonstrated a further increase in capillary density compared with AM or MNC alone. Contribution of transplanted MNC to neovascularization (the ratio of DAPI/PKH26 double-positive cells to lectin-positive cells) was significantly greater in the AM-MNC group than in the MNC group. A recent study (14) has reported that AM promotes proliferation and migration of human umbilical vein endothelial cells and enhances angiogenesis in a murine gel plug assay through the PI3-kinase/Akt pathway. We have also shown that intramuscular administration of AM DNA induces therapeutic angiogenesis in a rabbit model of chronic hindlimb ischemia via activation of Akt (24). These findings suggest that the beneficial effects of combination therapy using AM and MNC may be attributable, in part, to the angiogenic properties of AM itself. Thus it is possible that AM infusion and MNC transplantation induce additive effects on myocardial damage after myocardial infarction. However, it still remains unknown whether AM infusion plus MNC transplantation induces synergetic effects.

An earlier study has demonstrated that ischemia and mechanical stress induce apoptosis of transplanted cells in the early stage after MNC transplantation (9). These results raise the possibility that the angiogenic potency of MNC transplantation is attenuated by MNC apoptosis. Kim et al. (7) have demonstrated that AM inhibits apoptosis of endothelial cells through the PI3-kinase/Akt pathway in vitro. Activation of the PI3-kinase/Akt pathway has been shown to inhibit apoptosis of endothelial progenitor cells and enhance neovascularization (11). In the present study, AM infusion significantly inhibited MNC apoptosis in ischemic tissue. In vitro, we showed that the antiapoptotic effect of AM on MNC was mediated by activation of the PI3-kinase/Akt pathway. Thus AM may enhance the therapeutic potency of MNC transplantation through a direct action of AM on MNC survival. Moreover, immunohistological examination demonstrated that infusion of AM increased the number of lectin-positive (endothelial) cells in transplanted MNC. These findings raise the possibility that AM may enhance differentiation of MNC into the endothelial lineage. Thus AM may directly act on transplanted MNC, which may result in synergetic effects on the ischemic myocardium.

This study includes some study limitations. Although the labeling efficacy of PKH26 has been shown to persist for >8 wk without cell toxicity (3, 4), the used vital marker PKH26

may have some cell toxic effects and cell or membrane fusion can lead to labeling of neighboring cells in the target tissue. Second, the present study demonstrated that AM prolongs MNC survival through the PI3-kinase/Akt pathway and enhances neovascularization in a peri-infarcted area. However, further studies are necessary to examine the effect of AM on MNC differentiation into endothelial cells.

Autologous cell transplantation may be an alternative treatment for ischemic heart disease in the clinical setting. Because their use does not require immunosuppression, the clinical use of MNC for cellular cardiomyoplasty appears to be most advantageous. Administration of AM peptide is simple and relatively noninvasive. We and others (12, 16, 17) have reported the safety of AM infusion in humans. Thus combination therapy using AM infusion and MNC transplantation may be a new therapeutic strategy for the treatment of ischemic heart disease.

In conclusion, infusion of AM enhanced the angiogenic potency of MNC transplantation and improved cardiac function in rats with myocardial infarction. This beneficial effect may be mediated partly by the angiogenic property of AM itself and by its antiapoptotic effect on MNC. Thus combination therapy using AM infusion and MNC transplantation may be a new therapeutic strategy for the treatment of ischemic heart disease.

GRANTS

This work was supported by Ministry of Education, Culture, Sports, Science and Technology Grant-in-Aid for Scientific Research 13470154; Health and Labor Sciences Research Grants nano 001 and genome 005; Ministry of Health, Labor and Welfare Research Grant for Cardiovascular Disease H13C-1 and 16C-6; and grants from New Energy and Industrial Technology Development Organization and the Promotion of Fundamental Studies in Health Science of the Organization for Pharmaceutical Safety and Research of Japan.

REFERENCES

1. **Asahara T, Murohara T, Sullivan A, Silver M, van der Zee R, Li T, Witzenbichler B, Schatteman G, and Isner JM.** Isolation of putative progenitor endothelial cells for angiogenesis. *Science* 275: 964–967, 1997.
2. **Chien YW, Barbee RW, MacPhee AA, Frohlich ED, and Trippodo NC.** Increased ANF secretion after volume expansion is preserved in rats with heart failure. *Am J Physiol Regul Integr Comp Physiol* 254: R185–R191, 1988.
3. **Fox D, Kouris GJ, Blumofe KA, Heilizer TJ, Husak V, and Greisler HP.** Optimizing fluorescent labeling of endothelial cells for tracking during long-term studies of autologous transplantation. *J Surg Res* 86: 9–16, 1999.
4. **Gulbins H, Pritisanac A, Anderson I, Uhlig A, Goldemund A, Daebritz S, Meiser B, and Reichart B.** Myoblasts for survive 16 weeks after intracardiac transfer and start differentiation. *Thorac Cardiovasc Surg* 51: 295–300, 2003.
5. **Hennekens CH.** Increasing burden of cardiovascular disease: current knowledge and future directions for research on risk factors. *Circulation* 97: 1095–1102, 1998.
6. **Kamihata H, Matsubara H, Nishiue T, Fujiyama S, Tsutsumi Y, Ozono R, Masaki H, Mori Y, Iba O, Tateishi E, Kosaki A, Shintani S, Murohara T, Imaizumi T, and Iwasaka T.** Implantation of bone marrow mononuclear cells into ischemic myocardium enhances collateral perfusion and regional function via side supply of angioblasts, angiogenic ligands, and cytokines. *Circulation* 104: 1046–1052, 2001.
7. **Kim W, Moon SO, Sung MJ, Kim SH, Lee S, So JN, and Park SK.** Angiogenic role of adrenomedullin through activation of Akt, mitogen-activated protein kinase, and focal adhesion kinase in endothelial cells. *FASEB J* 17: 1937–1939, 2003.
8. **Kitamura K, Kangawa K, Kawamoto M, Ichiki Y, Nakamura S, Matsuo H, and Eto T.** Adrenomedullin: a novel hypotensive peptide isolated from human pheochromocytoma. *Biochem Biophys Res Commun* 192: 553–560, 1993.
9. **Kobayashi T, Hamano K, Li TS, Katoh T, Kobayashi S, Matsuzaki M, and Esato K.** Enhancement of angiogenesis by the implantation of self bone marrow cells in a rat ischemic heart model. *J Surg Res* 89: 189–195, 2000.
10. **Kocher AA, Schuster MD, Szabolcs MJ, Takuma S, Burkhoff D, Wang J, Homma S, Edwards NM, and Itescu S.** Neovascularization of ischemic myocardium by human bone-marrow-derived angioblasts prevents cardiomyocyte apoptosis, reduces remodeling and improves cardiac function. *Nat Med* 7: 430–436, 2001.
11. **Llevadot J, Murasawa S, Kureishi Y, Uchida S, Masuda H, Kawamoto A, Walsh K, Isner JM, and Asahara T.** HMG-CoA reductase inhibitor mobilizes bone marrow-derived endothelial progenitor cells. *J Clin Invest* 108: 399–405, 2001.
12. **McGregor DO, Troughton RW, Frampton C, Lynn KL, Yandle T, Richards AM, and Nicholls MG.** Hypotensive and natriuretic actions of adrenomedullin in subjects with chronic renal impairment. *Hypertension* 37: 1279–1284, 2001.
13. **Messina LM, Podrazik RM, Whitehill TA, Ekhterae D, Brothers TE, Wilson JM, Burkel WE, and Stanley JC.** Adhesion and incorporation of lacZ-transduced endothelial cells into the intact capillary wall in the rat. *Proc Natl Acad Sci USA* 89: 12018–12022, 1992.
14. **Miyashita K, Itoh H, Sawada N, Fukunaga Y, Sone M, Yamahara K, Yurugi-Kobayashi T, Park K, and Nakao K.** Adrenomedullin provokes endothelial Akt activation and promotes vascular regeneration both in vitro and in vivo. *FEBS Lett* 544: 86–92, 2003.
15. **Murohara T, Ikeda H, Duan J, Shintani S, Sasaki K, Eguchi H, Onitsuka I, Matsui K, and Imaizumi T.** Transplanted cord blood-derived endothelial precursor cells augment postnatal neovascularization. *J Clin Invest* 105: 1527–1536, 2000.
16. **Nagaya N, Kyotani S, Uematsu M, Ueno K, Oya H, Nakanishi N, Shirai M, Mori H, Miyatake K, and Kangawa K.** Effects of adrenomedullin inhalation on hemodynamics and exercise capacity in patients with idiopathic pulmonary hypertension. *Circulation* 109: 351–356, 2004.
17. **Nagaya N, Satoh T, Nishikimi T, Uematsu M, Furuichi S, Sakamaki F, Oya H, Kyotani S, Nakanishi N, Goto Y, Masuda Y, Miyatake K, and Kangawa K.** Hemodynamic, renal, and hormonal effects of adrenomedullin infusion in patients with congestive heart failure. *Circulation* 101: 498–503, 2000.
18. **Okumura H, Nagaya N, Itoh T, Okano I, Hino J, Mori K, Tsukamoto Y, Ishibashi-Ueda H, Miwa S, Tambara K, Toyokuni S, Yutani C, and Kangawa K.** Adrenomedullin infusion attenuates myocardial ischemia/reperfusion injury through the phosphatidylinositol 3-kinase/Akt-dependent pathway. *Circulation* 109: 242–248, 2004.
19. **Rafii S and Lyden D.** Therapeutic stem and progenitor cell transplantation for organ vascularization and regeneration. *Nat Med* 9: 702–712, 2003.
20. **Sata M, Kakoki M, Nagata D, Nishimatsu H, Suzuki E, Aoyagi T, Sugiura S, Kojima H, Nagano T, Kangawa K, Matsuo H, Omata M, Nagai R, and Hirata Y.** Adrenomedullin and nitric oxide inhibit human endothelial cell apoptosis via a cyclic GMP-independent mechanism. *Hypertension* 36: 83–88, 2000.
21. **Schiller NB, Shah PM, Crawford M, DeMaria A, Devereux R, Feigenbaum H, Gutgesell H, Reichek N, Sahn D, Schnittger I, Silverman NH, and Tajik AJ.** Recommendations for quantitation of the left ventricle by two-dimensional echocardiography. American Society of Echocardiography Committee on Standards, Subcommittee on Quantitation of Two-Dimensional Echocardiograms. *J Am Soc Echocardiogr* 2: 358–367, 1989.
22. **Shiojima I and Walsh K.** Role of Akt signaling in vascular homeostasis and angiogenesis. *Circ Res* 90: 1243–1250, 2002.
23. **Strauer BE, Brehm M, Zeus T, Kostering M, Hernandez A, Sorg RV, Kogler G, and Wernet P.** Repair of infarcted myocardium by autologous intracoronary mononuclear bone marrow cell transplantation in humans. *Circulation* 106: 1913–1918, 2002.
24. **Tokunaga N, Nagaya N, Shirai M, Tanaka E, Ishibashi-Ueda H, Harada-Shiba M, Kanda M, Ito T, Shimizu W, Tabata Y, Uematsu M, Nishigami K, Sano S, Kangawa K, and Mori H.** Adrenomedullin gene transfer induces therapeutic angiogenesis in a rabbit model of chronic hind limb ischemia: benefits of a novel nonviral vector, gelatin. *Circulation* 109: 526–531, 2004.
25. **Tse HF, Kwong YL, Chan JK, Lo G, Ho CL, and Lau CP.** Angiogenesis in ischaemic myocardium by intramyocardial autologous bone marrow mononuclear cell implantation. *Lancet* 361: 47–49, 2003.

Honorable Mention Poster Award

High-speed K-edge angiography achieved with tantalum K-series characteristic x rays

Eiichi Sato*[a], Etsuro Tanaka[b], Hidezo Mori[c], Toshiaki Kawai[d], Takashi Inoue[c], Akira Ogawa[c], Shigehiro Sato[f], Kazuyoshi Takayama[g] and Hideaki Ido[h]

[a] Department of Physics, Iwate Medical University, 3-16-1 Honchodori, Morioka 020-0015, Japan,
[b] Department of Nutritional Science, Faculty of Applied Bio-science, Tokyo University of Agriculture, 1-1-1 Sakuragaoka, Setagaya-ku 156-8502, Japan
[c] Department of Cardiac Physiology, National Cardiovascular Center Research Institute, 5-7-1 Fujishirodai, Suita, Osaka 565-8565, Japan
[d] Electron Tube Division #2, Hamamatsu Photonics K. K., 314-5 Shimokanzo, Toyooka Village, Iwata-gun 438-0193, Japan
[e] Department of Neurosurgery, School of Medicine, Iwate Medical University, 19-1 Uchimaru, Morioka 020-8505, Japan
[f] Department of Microbiology, School of Medicine, Iwate Medical University, 19-1 Uchimaru, Morioka 020-8505, Japan
[g] Shock Wave Research Center, Institute of Fluid Science, Tohoku University, 2-1-1 Katahira, Sendai 980-8577, Japan
[h] Department of Applied Physics and Informatics, Faculty of Engineering, Tohoku Gakuin University, 1-13-1 Chuo, Tagajo 985-8537, Japan

ABSTRACT

The tantalum plasma flash x-ray generator is useful in order to perform high-speed K-edge angiography using cone beams because Kα rays from the tantalum target are absorbed effectively by gadolinium-based contrast media. In the flash x-ray generator, a 150 nF condenser is charged up to 80 kV by a power supply, and flash x rays are produced by the discharging. The x-ray tube is a demountable diode, and the turbomolecular pump evacuates air from the tube with a pressure of approximately 1 mPa. Since the electric circuit of the high-voltage pulse generator employs a cable transmission line, the high-voltage pulse generator produces twice the potential of the condenser charging voltage. When the charging voltage was increased, the K-series characteristic x-ray intensities of tantalum increased. The K lines were clean and intense, and hardly any bremsstrahlung rays were detected. The x-ray pulse widths were approximately 100 ns, and the time-integrated x-ray intensity had a value of approximately 300 μGy at 1.0 m from the x-ray source with a charging voltage of 80 kV. Angiography was performed using a film-less computed radiography (CR) system and gadolinium-based contrast media. In angiography of non-living animals, we observed fine blood vessels of approximately 100 μm with high contrasts.

Keywords: angiography, gadolinium-based contrast media, characteristic x rays, quasi-monochromatic x rays, tantalum Kα photons

1. INTRODUCTION

The successful uses of monochromatic parallel beams from synchrotron orbital radiation in recent years have greatly increased the demand for phase-contrast radiography[1-3] and enhanced K-edge angiography.[4-6] In particular, the parallel beams with photon energies of approximately 35 keV have been employed to perform angiography, because the beams are absorbed effectively by iodine-based contrast media with a K-absorption edge of 33.2 keV. Without using a synchrotron, we have developed an x-ray generator utilizing a cerium-target tube, and have performed cone-beam K-edge angiography achieved with cerium Kα rays of 34.6 keV.[7] However, the x-ray intensity rate was limited because

Medical Imaging 2005: Physics of Medical Imaging, edited by Michael J. Flynn, Proceedings of SPIE Vol. 5745 (SPIE, Bellingham, WA, 2005)
1605-7422/05/$15 · doi: 10.1117/12.601547

the thermal contact between the target and the anode was not good.
Although various flash x-ray generators have been developed,[8] we have developed flash x-ray generators[9-13] with photon energies of less than 150 keV in order to primarily perform high-speed biomedical radiography. Subsequently, we have developed plasma flash x-ray generators[14-16] to perform a preliminary experiment for producing hard x-ray lasers from weakly ionized linear plasma, and have succeeded in producing intense and clean K-series characteristic x rays using copper and nickel targets. In addition, we have confirmed the weak hard x-ray resonation verified from irradiation of weakly higher harmonic x rays. However, it is difficult to produce high-photon-energy characteristic x rays because the plasma transmits high-photon-energy bremsstrahlung x rays. Therefore, we developed a quasi-monochromatic flash x-ray generator[17,18] with a disk-cathode tube to produce high-energy characteristic x rays utilizing the angle dependence of bremsstrahlung x-ray distribution, because the bremsstrahlung rays are not emitted in the apposite direction to that of electron acceleration. Using this generator, we have succeeded in producing clean characteristic x rays from molybdenum, silver and cerium targets.
Gadolinium-based contrast media with a K-edge of 50.2 keV have been employed to perform angiography in MRI, and the gadolinium density has been increasing. In view of this situation, ytterbium Kα rays (52.0 keV) are useful for enhanced K-edge angiography, because the Kα rays are absorbed effectively by gadolinium media. As compared with angiography using iodine media, the absorbed dose can be decreased considerably utilizing angiography achieved with gadolinium media. However, because ytterbium is a lanthanide series element and has a high reactivity, Kα rays of tantalum and tungsten are also useful to perform angiography.
In this article, we describe an intense quasi-monochromatic plasma flash x-ray generator with a tantalum target tube, and used it to perform a preliminary study on angiography achieved with tantalum K-series characteristic x rays.

2. PRINCIPLE OF K-EDGE ANGIOGRAPHY

Figure 1 shows the mass attenuation coefficients of gadolinium at the selected energies; the coefficient curve is discontinuous at the gadolinium K-edge. The average photon energy of the tantalum Kα lines is shown above the gadolinium K-edge. The average photon energy of tantalum Kα lines is 57.1 keV, and gadolinium contrast media with a K-absorption edge of 50.2 keV absorb the lines easily. Therefore, blood vessels were observed with high contrasts.

3. GENERATOR

3.1 High-voltage circuit

Figure 2 shows a block diagram of a high-intensity plasma flash x-ray generator. The generator consists of the following essential components: a high-voltage power supply, a high-voltage condenser with a capacity of approximately 150 nF, an air gap switch, a turbomolecular pump, a thyratron pulse generator as a trigger device, and a flash x-ray tube. In this generator, a coaxial cable transmission line is employed in order to increase maximum tube voltage using high-voltage reflection (Fig. 3). The high-voltage main condenser is charged up to 80 kV by the power supply, and electric charges in the condenser are discharged to the tube through the four cables after closing the gap switch with the trigger device.

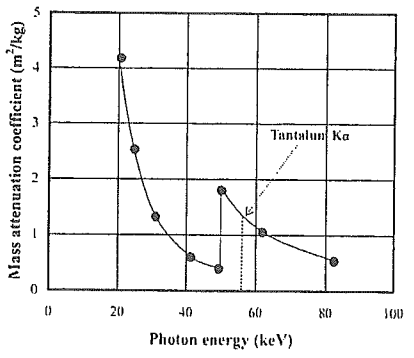

Figure 1: Relation between mass attenuation coefficient of gadolinium and average photon energy of tantalum Kα lines.

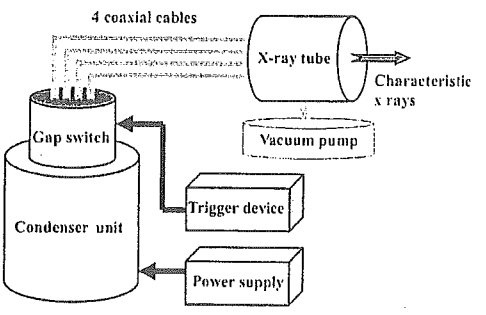

Figure 2: Block diagram of intense quasi-monochromatic flash x-ray generator.

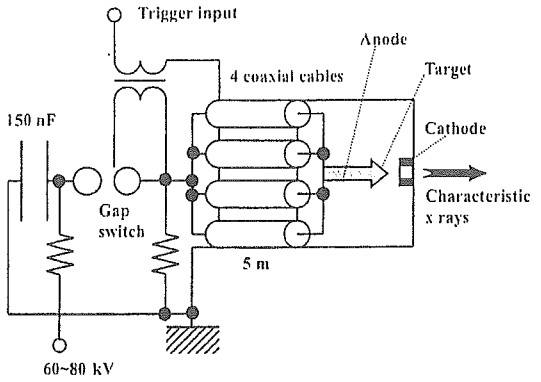

Figure 3: High-voltage circuit of flash x-ray generator.

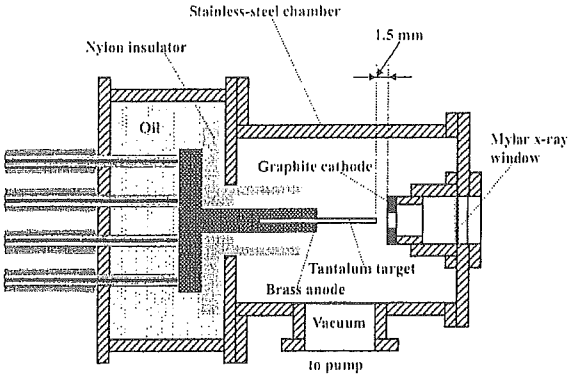

Figure 4: Schematic drawing of flash x-ray tube.

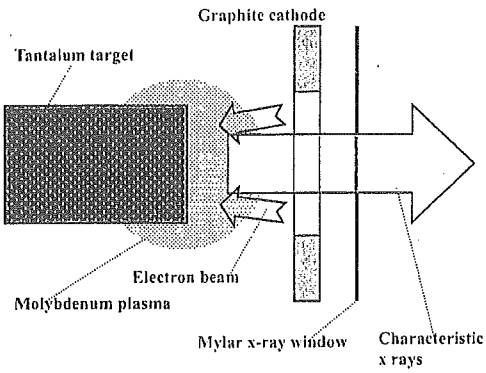

Figure 5: Irradiation of characteristic x rays.

3.2 X-ray tube

The x-ray tube is a demountable cold-cathode diode that is connected to the turbomolecular pump with a pressure of approximately 1 mPa (Fig. 4). This tube consists of the following major parts: a ring-shaped graphite cathode with an bore diameter of 4.5 mm, a stainless-steel vacuum chamber, a nylon insulator, a polyethylene terephthalate (Mylar) x-ray window 0.25 mm in thickness, and a rod-shaped tantalum target 3.0 mm in diameter. The distance between the target and cathode electrodes can be regulated from the outside of the tube, and is set to 1.5 mm. As electron beams from the cathode electrode are roughly converged to the target by the electric field in the tube, evaporation leads to the formation of weakly ionized plasma, consisting of tantalum ions and electrons, around the target. Because bremsstrahlung rays are not emitted in the opposite direction to that of electron acceleration (Fig. 5), tantalum K-series characteristic x rays can be produced without using a filter.

4. CHARACTERISTICS

4.1 Tube voltage and current

In this generator, it was difficult to measure the tube voltage and current since the tube voltages were high, and there was no space to set a current transformer for measuring the tube current. Currently, the voltage and current roughly display damped oscillations. When the charging voltage was increased, both the maximum tube voltage and current increased. At a charging voltage of 80 kV, the estimated maximum values of the tube voltage and current were approximately 160 kV (2 times the charging voltage) and 40 kA, respectively.

4.2 X-ray output

X-ray output pulse was detected using a combination of a plastic scintillator and a photomultiplier (Fig. 6). The x-ray pulse height substantially increased with corresponding increases in the charging voltage. The x-ray pulse widths were approximately 100 ns, and the time-integrated x-ray intensity measured by a thermoluminescence dosimeter (Kyokko TLD Reader 1500 having MSO-S elements without energy compensation) had a value of approximately 300 μGy at 1.0 m from the x-ray source with a charging voltage of 80 kV.

4.3 X-ray source

In order to observe the characteristic x-ray source, we employed a 100-μm-diameter pinhole camera and an x-ray film (Polaroid XR-7) (Fig. 7). When the charging voltage was increased, the plasma x-ray source grew, and both spot dimension and intensity increased. Because the x-ray intensity is the highest at the center of the spot, both the dimension and intensity decreased according to decreases in the pinhole diameter.

4.4 X-ray spectra

X-ray spectra were measured using a transmission-type spectrometer with a lithium fluoride curved crystal 0.5 mm in thickness. The x-ray intensities of the spectra were detected by an imaging plate of a computed radiography (CR) system[19] (Konica Regius 150) with a wide dynamic range, and relative x-ray intensity was calculated from Dicom original digital data corresponding to x-ray intensity; the data was scanned by Dicom viewer in the film-less CR system. Subsequently, the relative x-ray intensity as a function of the data was calibrated using a conventional x-ray generator, and we confirmed that the intensity was proportional to the exposure time. Figure 8 shows measured spectra from the tantalum target. We observed clean K-series lines, while bremsstrahlung rays were hardly detected. The characteristic x-ray intensity substantially increased with increases in the charging voltage.

5. ANGIOGRAPHY

The flash angiography was performed by a computed radiography (CR) system (Konica Regius 150)[19] at 1.2 m from the x-ray source, and the charging voltage was 80 kV.

Firstly, rough measurements of spatial resolution were made using wires. Figure 9 shows radiograms of tungsten wires coiled around a rod made of polymethyl methacrylate. Although the image contrast decreased somewhat with decreases in the wire diameter, due to blurring of the image caused by the sampling pitch of 87.5 μm, a 50 μm-diameter wire could be observed. Because the tungsten wires transmitted the characteristic x rays easily, low contrast radiograms were obtained.

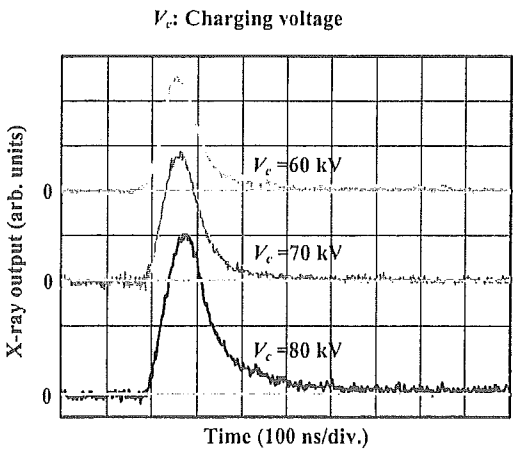

Figure 6: X-ray outputs at indicated conditions.

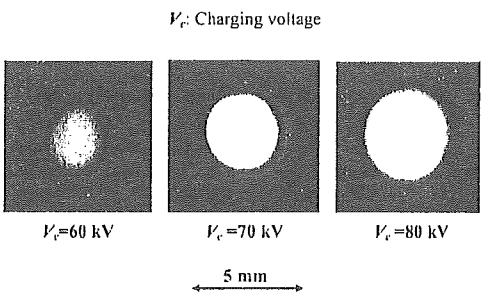

Figure 7: Images of characteristic x-ray source with changes in charging voltage.

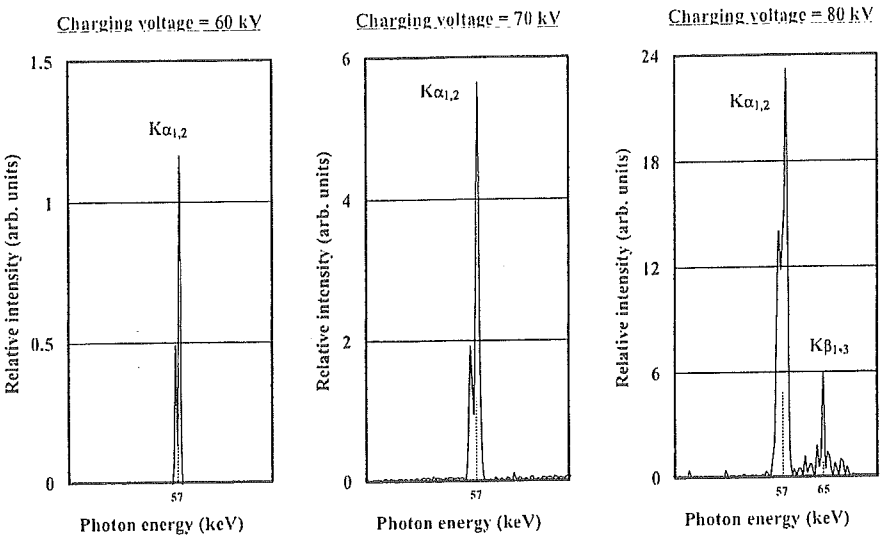

Figure 8: X-ray spectra from tantalum target.

The image of water (gadolinium oxide suspension of 20%) falling into a polypropylene beaker from a plastic test tube is shown in Fig. 10. The diameter of gadolinium oxide powder ranges from 1 to 10 μm. Because the x-ray duration was about 100 ns, the stop-motion image of water could be obtained.
Figure 11 shows an angiogram of a silicone rubber tube in a polymethyl methacrylate (PMMA) case using a contrast medium which contains 32.3% gadodiamidehydrate, and a low contrast tube with a bore diameter of 1.0 mm is observed. In cases where a gadolinium oxide suspension of 50% is employed, high-contrast angiography of the tubes (1.0 mm and 0.5 mm in bore diameter) could be performed (Fig. 12). Figure 13 shows an angiogram of a rabbit head using gadolinium oxide powder, and fine blood vessels of approximately 100 μm were visible.

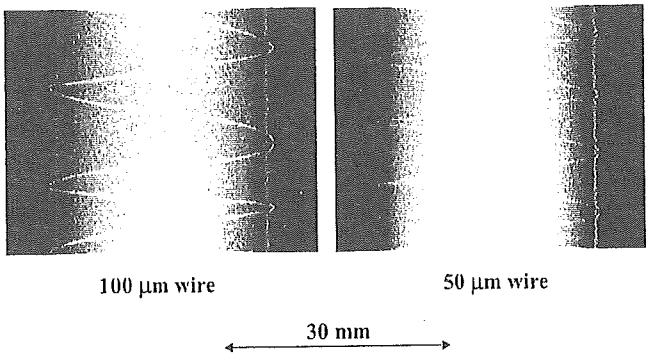

Figure 9: Radiograms of tungsten wires coiled around rod made of polymethyl methacrylate.

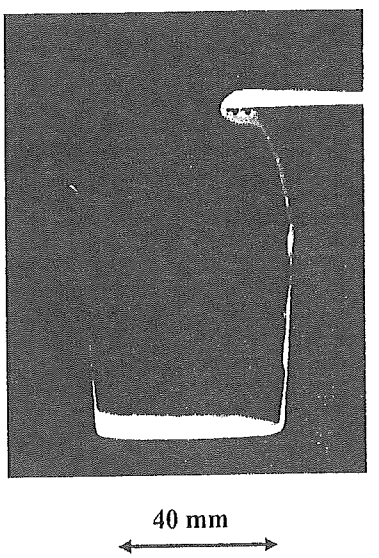

Figure 10: Radiogram of water falling into polypropylene beaker from plastic test tube.

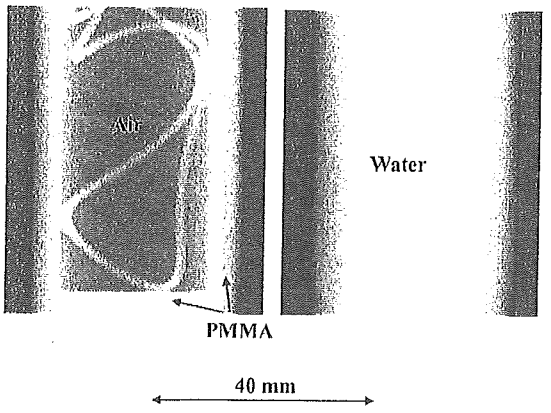

Figure 11: Angiograms of silicon tube using contrast medium of 32.3% gadodiamidehydrate.

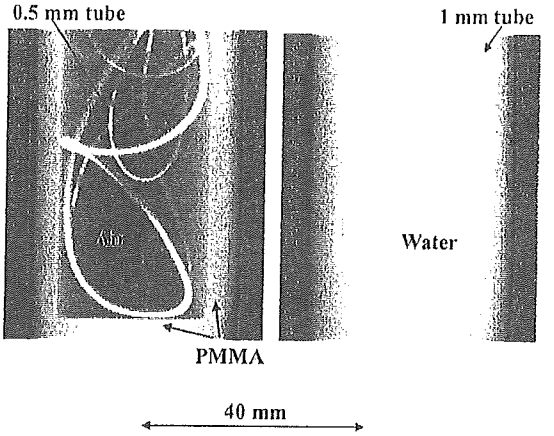

Figure 12: Angiography of silicon tube using gadolinium oxide suspension of 50%.

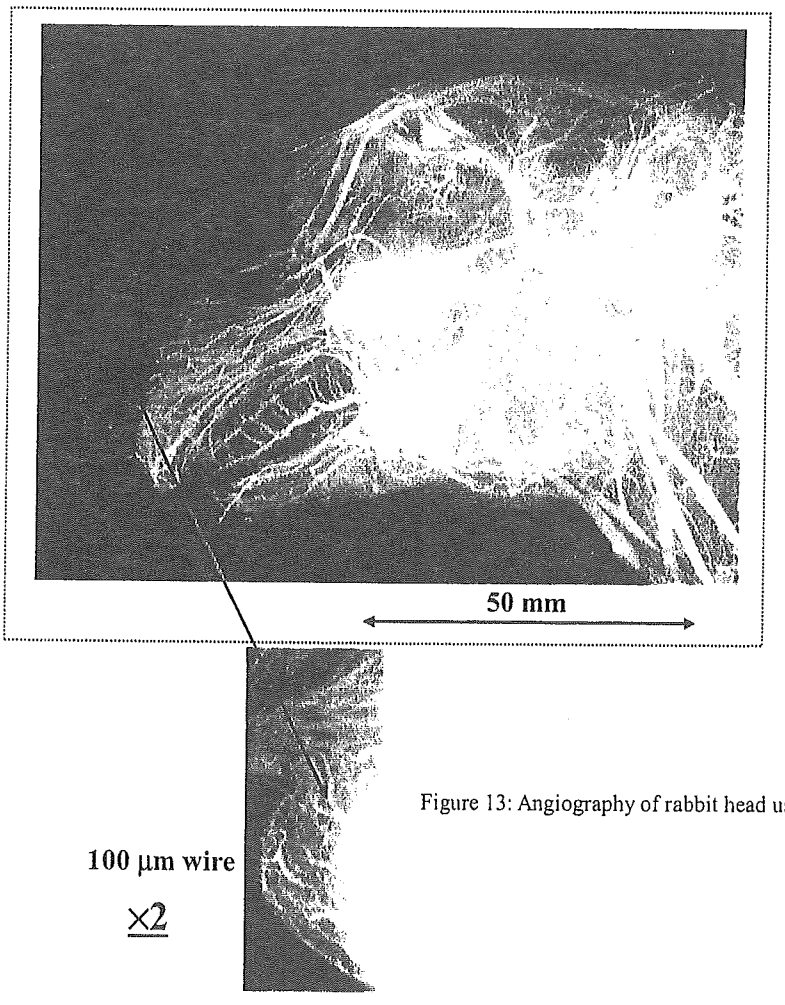

Figure 13: Angiography of rabbit head using gadolinium oxide powder.

6. DISCUSSION AND CONCLUSIONS

In summary, we succeeded in producing K-series characteristic x rays of tantalum and in performing K-edge angiography using gadolinium contrast media with a K-edge of 50.2 keV, and this K-edge angiography could be a useful technique to decrease the dose absorbed by patients. Although we employed tantalum Kα (57.1 keV) and Kβ (approximately 65 keV) rays, Kβ rays should be absorbed using an ytterbium oxide filter with an ytterbium K edge of 61.3 keV in order to increase the image contrast of blood vessels.

To perform K-edge angiography using gadolinium media, although an ytterbium target with a Kα energy of 52.0 keV is useful, the ytterbium has a high reactivity. If we assume that the ytterbium is employed, an alloy target should be developed. In this research, we obtained sufficient x-ray intensity per pulse for angiography, and the intensity can be increased by increasing the electrostatic energies in the high-voltage condenser. At a condenser capacity of 150 nF, the generator produced instantaneous number of K photons was approximately 1×10^9 photons/cm^2 per pulse at 1.0 m from the source.

In the flash x-ray tube, bremsstrahlung x rays with energies higher than the K-edge are absorbed effectively by the weakly ionized plasma and are converted into fluorescent (characteristic) x rays. In conjunction with this property, because the bremsstrahlung x rays are not emitted in the opposite direction to that of electron acceleration, clean characteristic x rays are produced. Using this flash x-ray generator, with which the photon energy of characteristic x rays can be selected, quasi-monochromatic imaging such as enhanced K-edge angiography using iodine contrast media and mammography can be performed.

ACKNOWLEDGMENT

This work was supported by Grants-in-Aid for Scientific Research (13470154, 13877114, 16591181, and 16591222) and Advanced Medical Scientific Research from MECSST, Health and Labor Sciences Research Grants(RAMT-nano-001, RHGTEFB-genome-005 and RHGTEFB-saisei-003), Grants from Keiryo Research Foundation, The Promotion and Mutual Aid Corporation for Private Schools of Japan, Japan Science and Technology Agency (JST), and New Energy and Industrial Technology Development Organization (NEDO, Industrial Technology Research Grant Program in '03).

REFERENCES

1. T. J. Davis, D. Gao, T. E. Gureyev, A. W. Stevenson and S. W. Wilkins, "Phase-contrast imagimg of weakly absorbing materials using hard x-rays," *Nature*, **373**, 595-597, 1995.

2. A. Momose, T. Takeda, Y. Itai and K. Hirano, "Phase-contrast x-ray computed tomography for observing biological soft tissues," *Nature Medicine*, **2**, 473-475, 1996.

3. M. Ando, A. Maksimenko, H. Sugiyama, W. Pattanasiriwisawa, K. Hyodo and C. Uyama, "A simple x-ray dark- and bright- field imaging using achromatic Laue optics," *Jpn. J. Appl. Phys.*, **41**, L1016-L1018, 2002.

4. A. C. Thompson, H. D. Zeman, G. S. Brown, J. Morrison, P. Reiser, V. Padmanabahn, L. Ong, S. Green, J. Giacomini, H. Gordon and E. Rubenstein, "First operation of the medical research facility at the NSLS for coronary angiography," *Rev. Sci. Instrum.*, **63**, 625-628, 1992.

5. H. Mori, K. Hyodo, E. Tanaka, M. U. Mohammed, A. Yamakawa, Y. Shinozaki, H. Nakazawa, Y. Tanaka, T. Sekka, Y. Iwata, S. Honda, K. Umetani, H. Ueki, T. Yokoyama, K. Tanioka, M. Kubota, H. Hosaka, N. Ishizawa and M. Ando, "Small-vessel radiography in situ with monochromatic synchrotoron radiation," *Radiology*, **201**, 173-177, 1996.

6. K. Hyodo, M. Ando, Y. Oku, S. Yamamoto, T. Takeda, Y. Itai, S. Ohtsuka, Y. Sugishita and J. Tada, "Development of a two-dimensional imaging system for clinical applications of intravenous coronary angiography using intense synchrotron radiation produced by a multipole wiggler," *J. Synchrotron Rad.*, **5**, 1123-1126, 1998.

7. E. Sato, E. Tanaka, H. Mori, T. Kawai, T. Ichimaru, S. Sato, K. Takayama and H. Ido, "Demonstration of enhanced K-edge angiography using a cerium target x-ray generator," *Med. Phys*, **31**, 3017-3021, 2004.

8. R. Germer, "X-ray flash techniques," *J. Phys. E: Sci. Instrum.*, **12**, 336-350, 1979.

9. E. Sato, S. Kimura, S. Kawasaki, H. Isobe, K. Takahashi, Y. Tamakawa and T. Yanagisawa, "Repetitive flash x-ray generator utilizing a simple diode with a new type of energy-selective function," *Rev. Sci. Instrum.*, **61**, 2343-2348, 1990.

10. A. Shikoda, E. Sato, M. Sagae, T. Oizumi, Y. Tamakawa and T. Yanagisawa, "Repetitive flash x-ray generator having a high-durability diode driven by a two-cable-type line pulser," *Rev. Sci. Instrum.*, **65**, 850-856, 1994.
11. E. Sato, K. Takahashi, M. Sagae, S. Kimura, T. Oizumi, Y. Hayasi, Y. Tamakawa and T. Yanagisawa, "Sub-kilohertz flash x-ray generator utilizing a glass-enclosed cold-cathode triode," *Med. & Biol. Eng. & Comput.*, **32**, 289-294, 1994.
12. K. Takahashi, E. Sato, M. Sagae, T. Oizumi, Y. Tamakawa and T. Yanagisawa, "Fundamental study on a long-duration flash x-ray generator with a surface-discharge triode," *Jpn. J. Appl. Phys.*, **33**, 4146-4151, 1994.
13. E. Sato, M. Sagae, K. Takahashi, A. Shikoda, T. Oizumi, Y. Hayasi, Y. Tamakawa and T. Yanagisawa, "10 kHz microsecond pulsed x-ray generator utilizing a hot-cathode triode with variable durations for biomedical radiography," *Med. & Biol. Eng. & Comput.*, **32**, 295-301, 1994.
14. E. Sato, Y. Hayasi, R. Germer, E. Tanaka, H. Mori, T. Kawai, H. Obara, T. Ichimaru, K. Takayama and H. Ido, "Irradiation of intense characteristic x-rays from weakly ionized linear molybdenum plasma," *Jpn. J. Med. Phys.*, **23**, 123-131, 2003.
15. E. Sato, Y. Hayasi, R. Germer, E. Tanaka, H. Mori, T. Kawai, T. Ichimaru, K. Takayama and H. Ido, "Quasi-monochromatic flash x-ray generator utilizing weakly ionized linear copper plasma," *Rev. Sci. Instrum.*, **74**, 5236-5240, 2003.
16. E. Sato, Y. Hayasi, R. Germer, E. Tanaka, H. Mori, T. Kawai, T. Ichimaru, S. Sato, K. Takayama and H. Ido, "Sharp characteristic x-ray irradiation from weakly ionized linear plasma," *J. Electron Spectrosc. Related Phenom.*, **137-140**, 713-720, 2004.
17. E. Sato, M. Sagae, E. Tanaka, Y. Hayasi, R. Germer, H. Mori, T. Kawai, T. Ichimaru, S. Sato, K. Takayama and H. Ido, "Quasi-monochromatic flash x-ray generator utilizing a disk-cathode molybdenum tube," *Jpn. J. Appl. Phys.*, **43**, 7324-7328, 2004.
18. E. Sato, E. Tanaka, H. Mori, T. Kawai, T. Ichimaru, S. Sato, K. Takayama and H. Ido, "Compact monochromatic flash x-ray generator utilizing a disk-cathode molybdenum tube," *Med. Phys.*, **32**, 49-54, 2005.
19. E. Sato, K. Sato and Y. Tamakawa, "Film-less computed radiography system for high-speed imaging," *Ann. Rep. Iwate Med. Univ. Sch. Lib. Arts and Sci.*, **35**, 13-23, 2000.

*dresato@iwate-med.ac.jp; phone +81-19-651-5111; fax +81-19-654-9282

High-speed enhanced K-edge angiography utilizing cerium plasma x-ray generator

Eiichi Sato, MEMBER SPIE
Iwate Medical University
Department of Physics
Morioka 020-0015, Japan
E-mail: dresato@iwate-med.ac.jp

Etsuro Tanaka
Tokyo University of Agriculture
Department of Nutritional Science
Faculty of Applied Bioscience
Setagaya-ku 156-8502, Japan

Hidezo Mori
National Cardiovascular Center Research Institute
Department of Cardiac Physiology
Osaka 565-8565, Japan

Toshiaki Kawai, MEMBER SPIE
Hamamatsu Photonics K. K.
Electron Tube Division #2
Iwata-gun 438-0193, Japan

Shigehiro Sato
Iwate Medical University
Department of Microbiology
School of Medicine
Morioka 020-8505, Japan

Kazuyoshi Takayama, MEMBER SPIE
Tohoku University
Shock Wave Research Center
Institute of Fluid Science
Sendai 980-8577, Japan

Abstract. The cerium target plasma flash x-ray generator is useful to perform high-speed enhanced K-edge angiography using cone beams, because K-series characteristic x-rays from the cerium target are absorbed effectively by iodine-based contrast mediums. In the plasma generator, a 200-nF condenser is charged up to 60 kV by a power supply, and flash x-rays are produced by the discharging. The x-ray tube is a demountable triode with a trigger electrode, and the turbomolecular pump evacuates air from the tube with a pressure of approximately 1 mPa. Target evaporation leads to the formation of weakly ionized linear plasma, consisting of cerium ions and electrons, around the target, and intense flash x-rays are produced. At a charging voltage of 55 kV, the maximum tube voltage is almost equal to the charging voltage of the main condenser, and the maximum current is approximately 20 kA. When the charging voltage is increased, weakly ionized cerium plasma forms, and the K-series characteristic x-ray intensities increase. The x-ray pulse widths are about 500 ns, and the time-integrated x-ray intensity has a value of about 40 μC/kg at 1.0 m from the x-ray source with a charging voltage of 55 kV. In the angiography, we employ a filmless computed radiography (CR) system and iodine-based microspheres.

[DOI: 10.1117/1.1882372]

Subject terms: plasma x-ray; cerium target; weakly ionized cerium plasma; characteristic x-ray; K-edge angiography.

Paper 040183 received Mar. 26, 2004; revised manuscript received Sep. 9, 2004; accepted for publication Oct. 25, 2004; published online Apr. 6, 2005. This paper is a revision of a paper presented at the SPIE conference on Ultrahigh- and High-Speed Photography, Photonics, and Videography, Aug. 2003, San Diego, California. The paper presented there appears (unrefereed) in SPIE Proceedings Vol. 5210.

1 Introduction

Flash x-rays are useful to perform high-speed radiography, and various generators have been developed to correspond to specific radiographic objectives.[1–5] In the cases of multishot and cine radiographies, we have developed several different repetitive-flash[6–10] and stroboscopic x-ray generators.[11–17] Although most flash x-ray generators have cold-cathode tubes, the stroboscopic generators utilize hot-cathode tubes.

In conjunction with single crystals, synchrotrons generate monochromatic x-rays. These rays play important roles in parallel radiography and have been employed to perform high-contrast K-edge angiography[18] and x-ray phase imaging.[19,20] However, it is difficult to obtain sufficient machine times for various research projects, including medical applications.

As for angiography using iodine-based contrast mediums, K-series characteristic x-rays of cerium are extremely useful, since the rays are absorbed easily by iodine. In particular, since fairly intense and sharp characteristic x-rays have been produced from weakly ionized linear plasmas[21–24] of nickel, copper, and molybdenum, the development of a cerium-target x-ray tube for angiography is highly desirable.

In this research, we developed a single flash x-ray generator with a cerium-target plasma tube and performed a preliminary study on weakly ionized cerium plasma angiography.

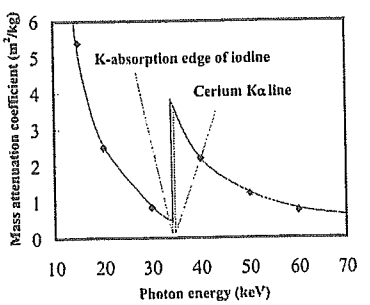

Fig. 1 Relation between mass attenuation coefficient of iodine and average photon energy of cerium Kα lines.

0091-3286/2005/$22.00 © 2005 SPIE

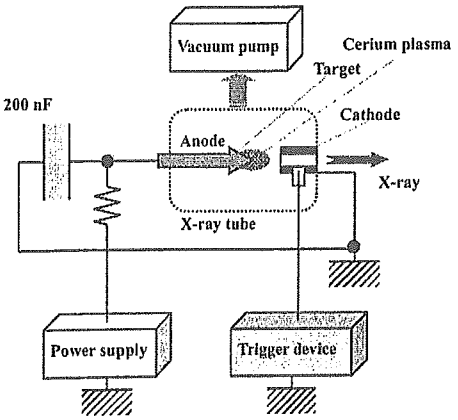

Fig. 2 Block diagram of high intensity plasma flash x-ray generator.

2 Principle of K-Edge Angiography

Figure 1 shows the mass attenuation coefficients of iodine at the selected energies; the coefficient curve is discontinuous at the iodine K-edge. The average photon energy of the cerium Kα lines is shown just above the iodine K-edge. Cerium is a rare earth element and has a high reactivity; however, the average photon energy of Kα lines is 34.566 keV, and iodine contrast mediums with a K-absorption edge of 33.155 keV absorb the lines easily. Therefore, blood vessels were observed with high contrasts.

3 Generator

3.1 *High-Voltage Circuit*

Figure 2 shows a block diagram of a high-intensity plasma flash x-ray generator. This generator consists of the following essential components: a high-voltage power supply, a high-voltage condenser with a capacity of about 200 nF, a turbomolecular pump, a krytron pulse generator as a trigger device, and a flash x-ray tube. The high-voltage main condenser is charged up to 60 kV by the power supply, and

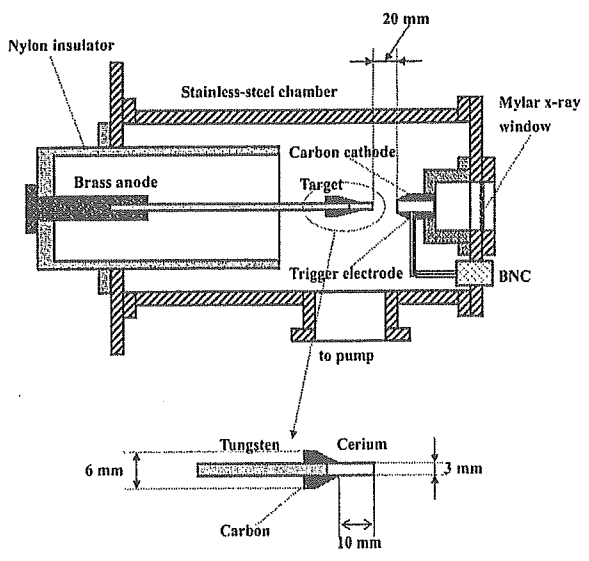

Fig. 3 Schematic drawing of flash x-ray tube.

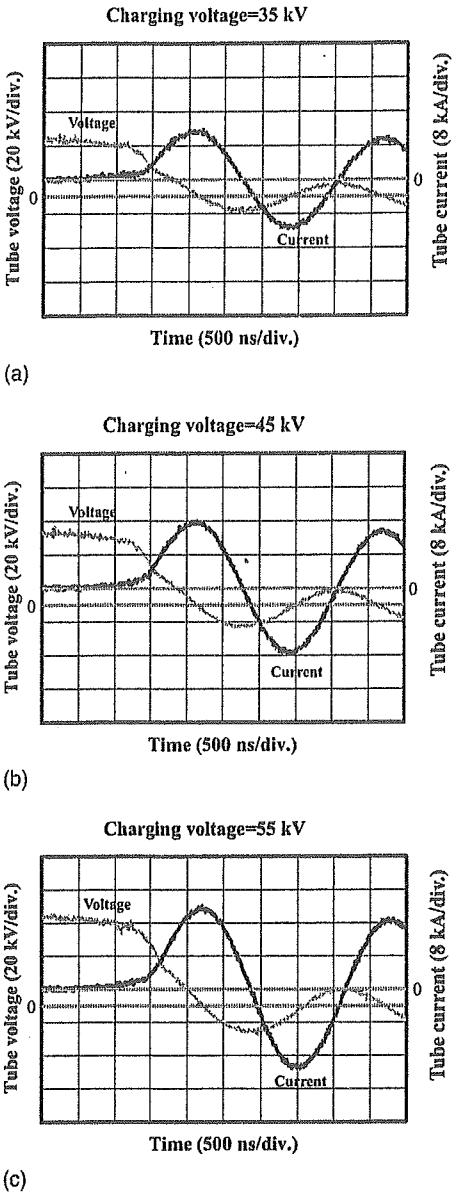

Fig. 4 Tube voltages and currents with charging voltage of (a) 35, (b) 45, and (c) 55 kV.

electric charges in the condenser are discharged to the tube after triggering the cathode electrode by the trigger device. The plasma flash x-rays are then produced.

3.2 *X-Ray Tube*

The x-ray tube is a demountable cold-cathode triode that is connected to the turbomolecular pump with a pressure of approximately 1 mPa (Fig. 3). This tube consists of the following major parts: a hollow cylindrical carbon cathode with a bore diameter of 10.0 mm, a trigger electrode made from a copper wire, a stainless-steel vacuum chamber, a nylon insulator, a polyethylene terephthalate (Mylar) x-ray window of 0.25 mm, and a rod-shaped cerium target of 3.0 mm in diameter. The target tip is embedded in the carbon rod to absorb the characteristic x-rays of carbon by the window. The distance between the target and cathode electrodes is approximately 20 mm, and the trigger electrode is

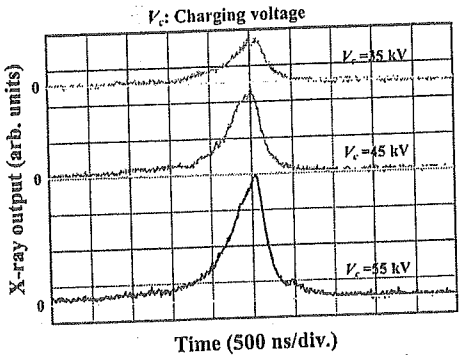

Fig. 5 X-ray outputs at indicated conditions.

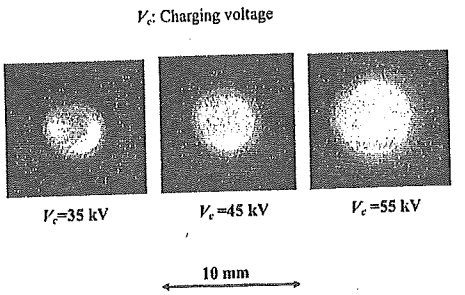

Fig. 6 Images of plasma x-ray source.

set in the cathode electrode. As electron beams from the cathode electrode are roughly converged to the target by an electric field in the tube, the weakly ionized plasma, which consists of cerium ions and electrons, forms around the target by evaporating.

4 Characteristics

4.1 *Tube Voltage and Current*

Tube voltage and current were measured by a high-voltage divider with an input impedance of 1 GΩ and a current transformer, respectively. Figure 4 shows the time relation between the tube voltage and current. At the indicated charging voltages, they roughly displayed damped oscillations. When the charging voltage was increased, both the maximum tube voltage and current increased. At a charging voltage of 55 kV, the maximum tube voltage was almost equal to the charging voltage of the main condenser, and the maximum tube current was about 20 kA.

4.2 *X-Ray Output*

An x-ray output pulse was detected using a combination of a plastic scintillator and a photomultiplier. The x-ray pulse height substantially increased with corresponding increases in the charging voltage (Fig. 5). The x-ray pulse widths were about 500 ns, and the time-integrated x-ray intensity measured by a thermoluminescence dosimeter (Kyokko TLD Reader 1500 utilizing MSO-S elements without energy compensation) had a value of about 40 μC/kg at 1.0 m from the x-ray source with a charging voltage of 55 kV.

4.3 *X-Ray Source*

To measure images of the plasma x-ray source, we employed a pinhole camera with a hole diameter of 100 μm (Fig. 6). When the charging voltage was increased, the plasma x-ray source grew, and both spot dimension and intensity increased. Because the x-ray intensity is the highest at the center of the spot, both the dimension and intensity decreased according to both increases in the thickness of a filter for absorbing x-rays and decreases in the pinhole diameter.

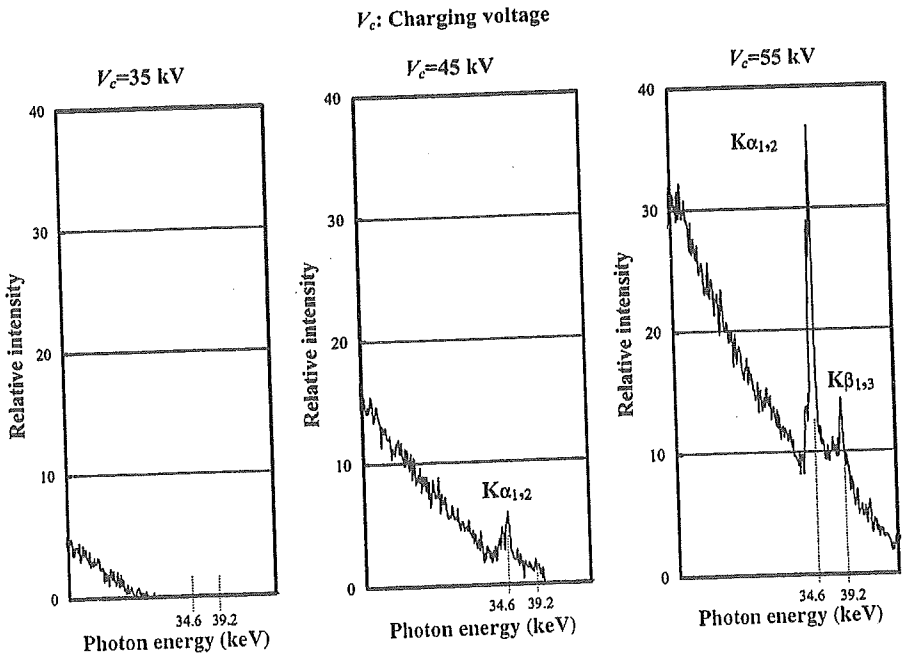

Fig. 7 X-ray spectra from weakly ionized cerium plasma.

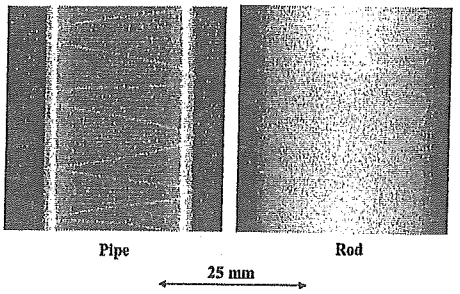

Fig. 8 Radiograms of tungsten wires of 50 μm in diameter coiled around pipe and rod made of PMMA.

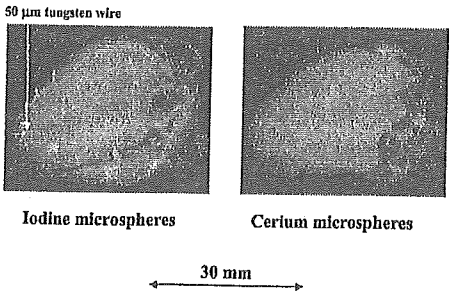

Fig. 10 Angiograms of rabbit hearts using iodine and cerium microspheres.

4.4 *X-Ray Spectra*

X-ray spectra from the plasma source were measured by a transmission-type spectrometer with a lithium fluoride curved crystal of 0.5 mm in thickness. The spectra were taken by a computed radiography (CR) system[25] (Konica Regius 150) having a wide dynamic range, and relative x-ray intensity was calculated from Dicom digital data. Figure 7 shows measured spectra from the cerium target. In this experiment, although we observed both the bremsstrahlung and characteristic x-rays, we could not observe characteristic x-rays with a charging voltage of 35 kV, because the critical excitation energy is 40.3 keV. Both intensities increased substantially with increases in the charging voltage.

5 Angiography

The plasma angiography was performed by the CR system without using a monochromatic filter, and the distance between the x-ray source and the imaging plate was 1.2 m.

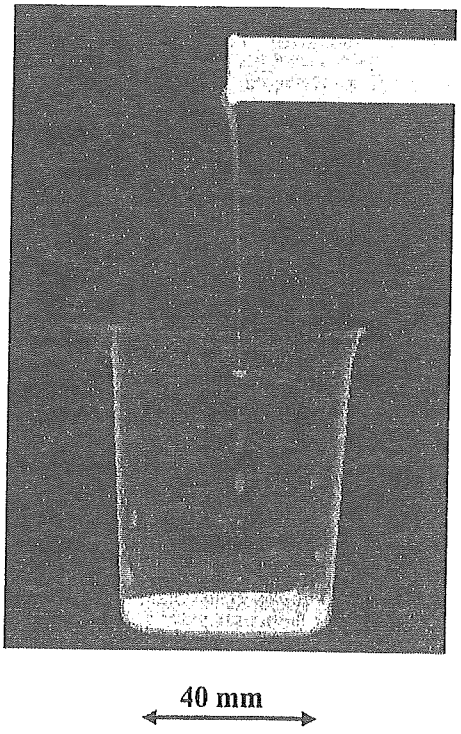

Fig. 9 Radiogram of water falling into a polypropylene beaker from a glass test tube.

Subsequently, in angiography testing, we usually employ nonliving animal phantoms using microspheres.

First, rough measurements of image resolution were made using wires. Figure 8 shows radiograms of 50-μm-diam tungsten wires coiled around a pipe, and a rod made of polymethyl methacrylate (PMMA) with a charging voltage of 55 kV. Although the image contrast increased using the pipe, 50-μm-diam wires could be observed.

The image of water falling into a polypropylene beaker from a glass test tube is shown in Fig. 9. This image was taken with a charging voltage of 55 kV, with the slight addition of an iodine-based contrast medium. Because the x-ray duration was about 1 μs, the stop-motion image of water could be obtained.

Angiograms of rabbit hearts are shown in Fig. 10. These two images were obtained using iodine and cerium microspheres of 15 μm, respectively, with a charging voltage of 55 kV. In cases where the cerium spheres were employed, the coronary arteries were barely visible. Figure 11 shows an angiogram of the external ear of a rabbit using iodine spheres with a charging voltage of 55 kV, and fine blood vessels of about 50 μm are visible. In angiography of a larger heart extracted from a dog, using iodine spheres, a PMMA plate was set in front of a heart facing x-ray source, and image contrast of coronary arteries improved with increases in the plate thickness (Fig. 12).

6 Discussion

In an earlier experiment using a copper target,[24] bremsstrahlung x-rays were hardly observed at all, and we confirmed the irradiation of fairly clean K-series characteristic x-rays such as lasers. In the present work, although we confirmed intense characteristic x-rays with a higher charging voltage, bremsstrahlung x-rays were detected, since the bremsstrahlung intensity is proportional to the atomic num-

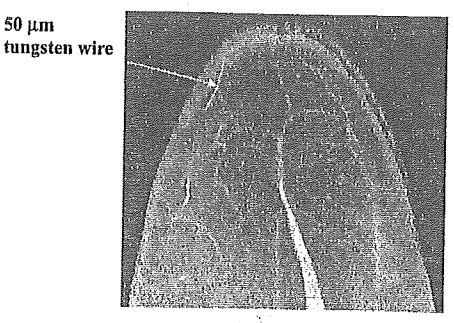

Fig. 11 Angiograms of external ear of rabbit.

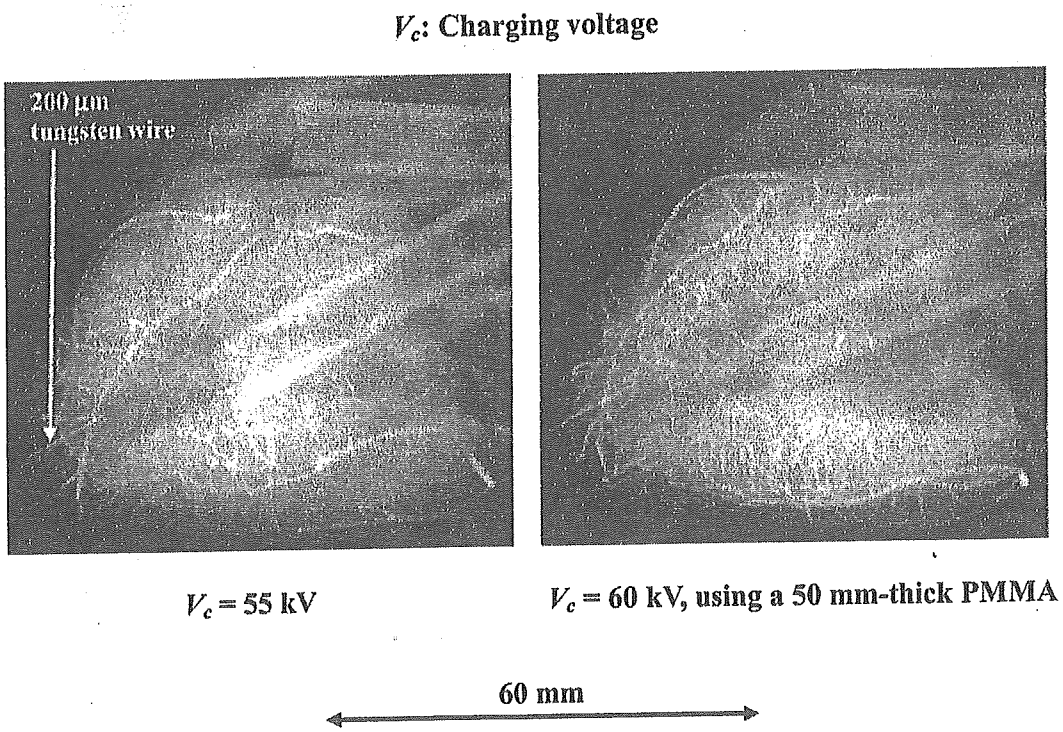

Fig. 12 Angiograms of extracted heart of dog.

ber of the target element, and high-photon-energy bremsstrahlung x-rays are not absorbed effectively in the plasma. Therefore, the condenser charging voltage should be raised as high as possible to increase the characteristic x-ray intensity. To decrease emission of bremsstrahlung x-rays from the carbon target holder, the target length should also be set as long as possible. Next, since the spheres easily transmit bremsstrahlung x-rays with energies lower than the edge, it is important that the rays be absorbed as much as possible before angiography to increase the image contrast.

In this research, we obtained sufficient x-ray intensity per pulse for CR radiography, and the generator produced high-dose-rate plasma x-rays of approximately 80 C/kg·s at 1.0 m with a charging voltage of 55 kV. In addition, because the x-ray intensity increases with increases in the electrostatic energy in the main discharge condenser, the flash x-rays from weakly ionized linear cerium plasma can be employed to perform high-speed angiography for cardiovascular disease.

Acknowledgments

This work was supported by Grants-in-Aid for Scientific Research (13470154, 13877114, and 16591222) and Advanced Medical Scientific Research from MECSST; Health and Labor Sciences Research Grants (RAMT-nano-001, RHGTEFB-genome-005, and RHGTEFB-saisei-003); and grants from Keiryo Research Foundation, The Promotion and Mutual Aid Corporation for Private Schools of Japan, Japan Science and Technology Agency (JST), and New Energy and Industrial Technology Development Organization (NEDO, Industrial Technology Research Grant Program in '03).

References

1. A. Mattsson, "Some characteristics of a 600 kV flash x-ray tube," *Phys. Scr.* **5**, 99–102 (1972).
2. R. Germer, "X-ray flash techniques," *J. Phys. E* **12**, 336–350 (1979).
3. E. Sato, H. Isobe, and F. Hoshino, "High intensity flash x-ray apparatus for biomedical radiography," *Rev. Sci. Instrum.* **57**, 1399–1408 (1986).
4. E. Sato, M. Sagae, K. Takahashi, T. Oizumi, H. Ojima, K. Takayama, Y. Tamakawa, T. Yanagisawa, A. Fujiwara, and K. Mitoya, "High-speed soft x-ray generators in biomedicine," *Proc. SPIE* **2513**, 649–667 (1994).
5. E. Sato, M. Sagae, A. Shikoda, K. Takahashi, T. Oizumi, M. Yamamoto, A. Takabe, K. Sakamaki, Y. Hayasi, H. Ojima, K. Takayama, and Y. Tamakawa, "High-speed soft x-ray techniques," *Proc. SPIE* **2869**, 937–955 (1996).
6. E. Sato, S. Kimura, S. Kawasaki, H. Isobe, K. Takahashi, Y. Tamakawa, and T. Yanagisawa, "Repetitive flash x-ray generator utilizing a simple diode with a new type of energy-selective function," *Rev. Sci. Instrum.* **61**, 2343–2348 (1990).
7. S. Kimura, E. Sato, M. Sagae, A. Shikoda, T. Oizumi, K. Takahashi, Y. Tamakawa, and T. Yanagisawa, "Disk-cathode flash x-ray tube driven by a repetitive two-stage Marx pulser," *Med. Biol. Eng. Comput.* **31**, S37–S43 (1993).
8. A. Shikoda, E. Sato, M. Sagae, T. Oizumi, Y. Tamakawa, and T. Yanagisawa, "Repetitive flash x-ray generator having a high-durability diode driven by a two-cable-type line pulser," *Rev. Sci. Instrum.* **65**, 850–856 (1994).
9. E. Sato, K. Takahashi, M. Sagae, S. Kimura, T. Oizumi, Y. Hayasi, Y. Tamakawa, and T. Yanagisawa, "Sub-kilohertz flash x-ray generator utilizing a glass-enclosed cold-cathode triode," *Med. Biol. Eng. Comput.* **32**, 289–294 (1994).
10. K. Takahashi, E. Sato, M. Sagae, T. Oizumi, Y. Tamakawa, and T. Yanagisawa, "Fundamental study on a long-duration flash x-ray generator with a surface-discharge triode," *Jpn. J. Appl. Phys.* **33**, 4146–4151 (1994).
11. E. Sato, A. Shikoda, S. Kimura, M. Sagae, H. Isobe, Y. Tamakawa, and T. Yanagisawa, "Kilohertz-range flash x-ray generator utilizing a triode in conjunction with an extremely hot cathode," *Rev. Sci. Instrum.* **62**, 2115–2120 (1991).
12. E. Sato, M. Sagae, K. Takahashi, A. Shikoda, T. Oizumi, Y. Hayasi, Y. Tamakawa, and T. Yanagisawa, "10 kHz microsecond pulsed x-ray generator utilizing a hot-cathode triode with variable durations for biomedical radiography," *Med. Biol. Eng. Comput.* **32**, 295–301 (1994).
13. E. Sato, T. Ichimaru, T. Usuki, K. Sato, H. Ojima, K. Takayama, H.

Ido, K. Sakamaki, and Y. Tamakawa, "Condenser-discharge stroboscopic x-ray generator SX-C98," *Proc. SPIE* **3516**, 618–625 (1998).
14. E. Sato, T. Ichimaru, H. Ojima, K. Takayama, H. Ido, and Y. Tamakawa, "Characteristics of the kilohertz-range harder stroboscopic x-ray generator and applications," *Proc. SPIE* **3771**, 12–21 (1999).
15. E. Sato, T. Ichimaru, H. Obara, M. Zuguchi, H. Mori, E. Tanaka, T. Usuki, K. Sato, H. Ojima, K. Takayama, K. Sakamaki, and Y. Tamakawa, "Condenser-discharge stroboscopic x-ray generator for medical radiography," *Proc. SPIE* **4183**, 383–393 (2000).
16. E. Sato, H. Ojima, K. Takayama, M. Matsumasa, H. Obara, M. Zuguchi, T. Usuki, K. Sato, K. Sakamaki, and Y. Tamakawa, "Observation of cavitation bubble cloud using a stroboscopic x-ray generator," *Proc. SPIE* **4183**, 394–404 (2000).
17. E. Sato, Y. Hayasi, and Y. Tamakawa, "Recent stroboscopic x-ray generators and their applications to high-speed radiography," *Ann. Rep. Iwate Med. Univ. Lib. Arts and Sci.* **35**, 1–11 (2000).
18. H. Mori, K. Hyodo, E. Tanaka, M. U. Mohammed, A. Yamakawa, Y. Shinozaki, H. Nakazawa, Y. Tanaka, T. Sekka, Y. Iwata, S. Honda, K. Umetani, H. Ueki, T. Yokoyama, K. Tanioka, M. Kubota, H. Hosaka, N. Ishizawa, and M. Ando, "Small-vessel radiography in situ with monochromatic synchrotoron radiation," *Radiology* **201**, 173–177 (1996).
19. T. J. Davis, D. Gao, T. E. Gureyev, A. W. Stevenson, and S. W. Wilkims, "Phase-contrast imaging of weakly absorbing materials using hard x-rays," *Nature (London)* **373**, 595–597 (1995).
20. A. Momose, T. Takeda, Y. Itai, and K. Hirano, "Phase-contrast x-ray computed tomography for observing biological soft tissues," *Nat. Med.* **2**, 473–475 (1996).
21. E. Sato, Y. Hayasi, E. Tanaka, H. Mori, T. Kawai, T. Usuki, K. Sato, H. Obara, T. Ichimaru, K. Takayama, H. Ido, and Y. Tamakawa, "Quasi-monochromatic radiography using a high-intensity quasi-x-ray laser generator," *Proc. SPIE* **4682**, 538–548 (2002).
22. E. Sato, Y. Hayasi, R. Germer, E. Tanaka, H. Mori, T. Kawai, H. Obara, T. Ichimaru, K. Takayama, and H. Ido, "Intense characteristic x-ray irradiation from weakly ionized linear plasma and applications," *Jpn. J. Med. Imag. Inform. Sci.* **20**, 148–155 (2003).
23. E. Sato, Y. Hayasi, R. Germer, E. Tanaka, H. Mori, T. Kawai, H. Obara, T. Ichimaru, K. Takayama, and H. Ido, "Irradiation of intense characteristic x-rays from weakly ionized linear molybdenum plasma," *Jpn. J. Med. Phys.* **23**, 123–131 (2003).
24. E. Sato, Y. Hayasi, R. Germer, E. Tanaka, H. Mori, T. Kawai, T. Ichimaru, K. Takayama, and Hideaki Ido, "Quasi-monochromatic flash x-ray generator utilizing weakly ionized linear copper plasma," *Rev. Sci. Instrum.* **74**, 5236–5240 (2003).
25. E. Sato, K. Sato, and Y. Tamakawa, "Film-less computed radiography system for high-speed Imaging," *Ann. Rep. Iwate Med. Univ. Sch. Lib. Arts Sci.* **35**, 13–23 (2000).

Eiichi Sato received his BS, MS, and PhD in applied physics from Tohoku Gakuin University, Sendai, Japan, in 1979, 1982, and 1987, respectively. From 1982, he was an assistant in the Department of Physics, and became an associate professor in 1986. Since 2004, he has been a professor of physics at Iwate Medical University. He has written some 400 publications and delivered some 200 international presentations concerning x-rays. His research interests include soft flash x-ray generators, quasi-x-ray laser generators, and high-speed radiography. In 2000 he received the Schardin Gold Medal from the German Physical Society, and in 2003 he received the Takayama Award (Gold Medal) from the Japan Society of High Speed Photography and Photonics.

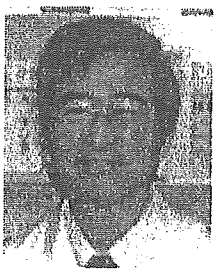

Etsuro Tanaka received his MD and PhD degrees in medicine from Kumamoto University, Japan, in 1980 and 1986, respectively. He worked on medical image processing in the Department of Physiology, Tokai University, Japan, from 1988 to 2003. He is currently a professor in the Department of Nutritional Sciences, Tokyo University of Agriculture, Japan. His research interests include medical image processing, human physiology, and clinical nutrition.

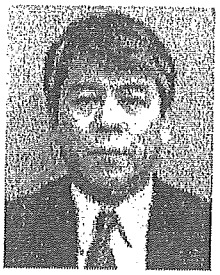

Hidezo Mori received a medical degree from Keio University School of Medicine, Tokyo, Japan, in 1977, and also a PhD from the Post Graduate School, Keio University School of Medicine. Now he is the director of the Department of Cardiac Physiology at the National Cardiovascular Center, Suita, Japan. His primary research interests are regenerative therapy in cardiovascular disease, microcirculation, and medical applications of structural biology.

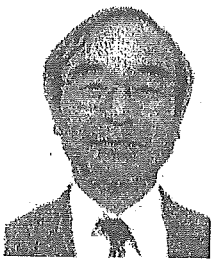

Toshiaki Kawai received the BS degree in precision mechanics and the MS degree in electronic engineering from Shizuoka University, Hamamatsu, Japan, in 1964 and 1974, respectively. In 1974, he joined the Hamamatsu Photonics K.K., where he worked on research and development of solid-state infrared detectors, and then from 1978 to 1981 engaged in research work on the NEA cold cathode for application to imaging camera tubes. He is now the project coordinator of the Electron Tube Division #2 and is engaged in the development and manufacturing of imaging devices and x-ray equipment. He is a member of the Japan Radioisotope Association and the Institute of Image Information and Television Engineers of Japan.

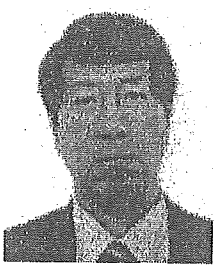

Shigehiro Sato received his MD degree from Iwate Medical University in 1980. He worked for the laboratory of the Division of Pediatric Infectious Diseases at Johns Hopkins Hospital from 1985 to 1989. He is currently a professor in the Department of Microbiology at Iwate Medical University. His research interests include central nervous system damage caused by Vero toxin, a cell culture system for vaccine development, and microangiography.

Kazuyoshi Takayama received his BS degree from Nagoya Institute of Technology in 1962. In 1970, he received his PhD in mechanical engineering from Tohoku University. Since 1986, he has been a director (professor) of the Shock Wave Research Center, Institute of Fluid Science, Tohoku University. His research interests include various shock wave phenomena, high-speed photography, and flash radiography. He has received seven awards including the coveted Ernst Mach Medal in 2000.

Clean monochromatic x-ray irradiation from weakly ionized linear copper plasma

Eiichi Sato, MEMBER SPIE
Iwate Medical University
Department of Physics
Morioka 020-0015, Japan
E-mail: dresato@iwate-med.ac.jp

Etsuro Tanaka
Tokyo University of Agriculture
Department of Nutritional Science
Faculty of Applied Bioscience
Setagaya-ku 156-8502, Japan

Hidezo Mori
National Cardiovascular Center Research Institute
Department of Cardiac Physiology
Osaka 565-8565, Japan

Toshiaki Kawai, MEMBER SPIE
Hamamatsu Photonics K.K.
Electron Tube Division #2
Iwata-gun 438-0193, Japan

Shigehiro Sato
Iwate Medical University
Department of Microbiology
School of Medicine
Morioka 020-8505, Japan

Kazuyoshi Takayama, MEMBER SPIE
Tohoku University
Shock Wave Research Center
Institute of Fluid Science
Sendai 980-8577, Japan

Abstract. In the plasma flash x-ray generator, a 200-nF condenser is charged up to 50 kV by a power supply, and flash x-rays are produced by the discharging. The x-ray tube is a demountable triode with a trigger electrode, and the turbomolecular pump evacuates air from the tube with a pressure of approximately 1 mPa. Target evaporation leads to the formation of weakly ionized linear plasma, consisting of copper ions and electrons, around the fine target, and intense Kα rays are produced using a 10-μm-thick nickel filter. At a charging voltage of 50 kV, the maximum tube voltage is almost equal to the charging voltage of the main condenser, and the peak current is about 15 kA. When the charging voltage is increased, the linear plasma forms, and the copper Kα intensities substantially increase. The Kα lines are quite clean and intense, and hardly any bremsstrahlung rays are detected at all. The x-ray pulse widths are approximately 700 ns, and the time-integrated x-ray intensity has a value of approximately 20 μC/kg at 1.0 m from the x-ray source with a charging voltage of 50 kV. [DOI: 10.1117/1.1882373]

Subject terms: flash x-ray; weakly ionized linear plasma; copper target; Kα characteristic x-rays; monochromatic x-rays.

Paper 040184 received Mar. 29, 2004; revised manuscript received Sep. 9, 2004; accepted for publication Oct. 25, 2004; published online Mar. 30, 2005. This paper is a revision of a paper presented at SPIE conference on Laser-Generated and Other Laboratory X-Ray and EUV Sources, Optics, and Applications, Aug. 2003, San Diego, California. The paper presented there appears (unrefereed) in SPIE Proceedings Vol. 5196.

1 Introduction

Flash x-rays have been produced by several different methods, and various generators have been developed corresponding to specific radiographic objectives.[1–3] Currently, maximum photon energy has been increased to approximately 1 MeV using multistage Marx pulse generators[1,2] to produce hard x-rays for military studies. In soft x-ray generators,[4–7] high-intensity single generators with large capacity condensers were originally developed. Subsequently, repetitive generators[8–12] have been developed, and the repetition rate has been increased to subkilohertz using a cold-cathode triode.

Recently, soft x-ray lasers have been produced by a gas-discharge capillary,[13–16] and the laser pulse energy substantially increased in proportion to the capillary length. These kinds of fast discharges can generate hot and dense plasma columns with aspect ratios approaching 1000:1. However, it is difficult to increase the laser photon energy to 10 keV or beyond. Because there are no x-ray resonators in the high photon energy region, new methods for increasing coherence will be desired in the future.

0091-3286/2005/$22.00 © 2005 SPIE

We have developed several different plasma flash x-ray generators corresponding to specific radiographic objectives, and a major goal in our research is the development of an intense and clean monochromatic x-ray generator that can impact applications with biomedical radiography. By forming weakly ionized linear plasma,[17–20] because we have succeeded in producing fairly intense and clean quasi-monochromatic x-rays from the plasma axial direction, monochromatic x-rays should be produced using a K-edge filter.

We describe a plasma flash x-ray generator utilizing a new plasma x-ray tube, and used it to perform a preliminary experiment for generating clean monochromatic x-rays by forming a linear copper plasma cloud around a fine target.

2 Generator

2.1 *High-Voltage Circuit*

Figure 1 shows a block diagram of the high-intensity plasma flash x-ray generator. This generator consists of the following essential components: a high-voltage power supply, a high-voltage condenser with a capacity of approximately 200 nF, a turbomolecular pump, a krytron pulse

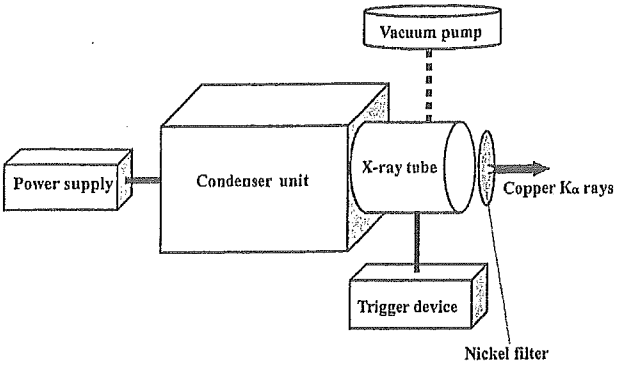

Fig. 1 Block diagram of high-intensity plasma flash x-ray generator.

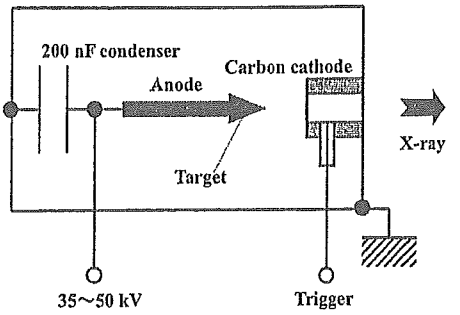

Fig. 2 Circuit diagram of generator.

generator as a trigger device, and a flash x-ray tube. In this generator, a low-impedance transmission line (Fig. 2) is employed to increase maximum tube current. The high-voltage main condenser is charged to 50 kV by the power supply, and electric charges in the condenser are discharged to the tube after triggering the cathode electrode with the trigger device. The plasma flash x-rays are then produced.

2.2 *X-Ray Tube*

The x-ray tube is a demountable cold cathode triode that is connected to the turbomolecular pump with a pressure of approximately 1 mPa (Fig. 3). This tube consists of the following major parts: a hollow cylindrical carbon cathode with a bore diameter of 10.0 mm, a brass focusing electrode, a trigger electrode made from copper wire, a stainless-steel vacuum chamber, a nylon insulator, a polyethylene terephthalate (Mylar) x-ray window 0.25 mm thick, and a rod-shaped copper target 3.0 mm in diameter with a tip angle of 60 deg. The distance between the target and cathode electrodes is approximately 20 mm, and the trigger electrode is set in the cathode electrode. As electron beams from the cathode electrode are roughly converged to the target by the focusing electrode, evaporation leads to the formation of a weakly ionized linear plasma, consisting of copper ions and electrons, around the fine target.

2.3 *Principle of Clean Kα-Ray Irradiation*

In the linear plasma, bremsstrahlung photons with energies higher than the K-absorption edge are effectively absorbed and are converted into fluorescent x-rays (Fig. 4). The plasma then transmits the fluorescent rays easily, and bremsstrahlung rays with energies lower than the K edge are also absorbed by the plasma. In addition, because bremsstrahlung rays are not emitted in the opposite direction to that of electron acceleration, intense characteristic x-rays are generated from the plasma-axial direction. Sub-

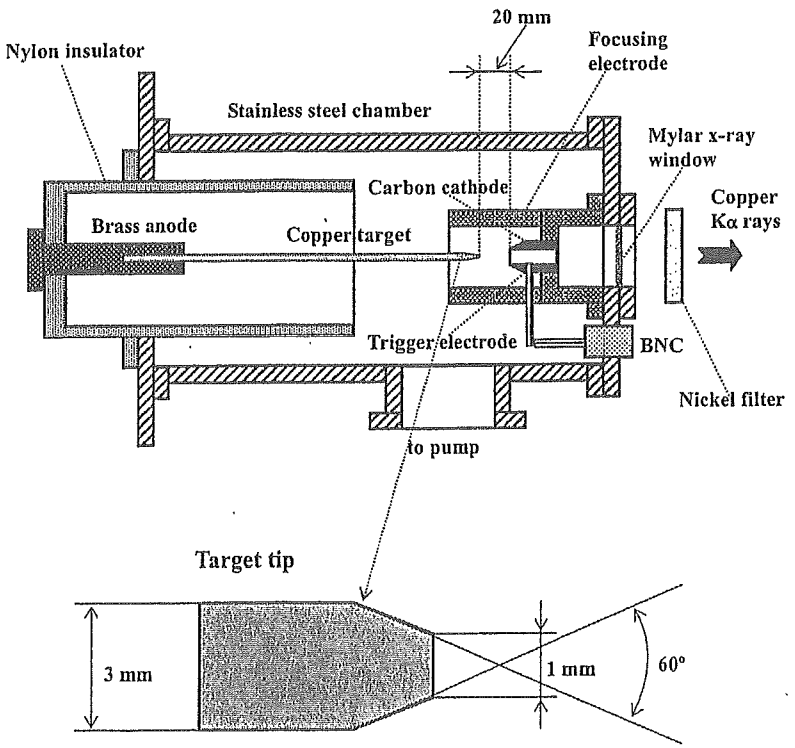

Fig. 3 Schematic drawing of flash x-ray tube with rod target.

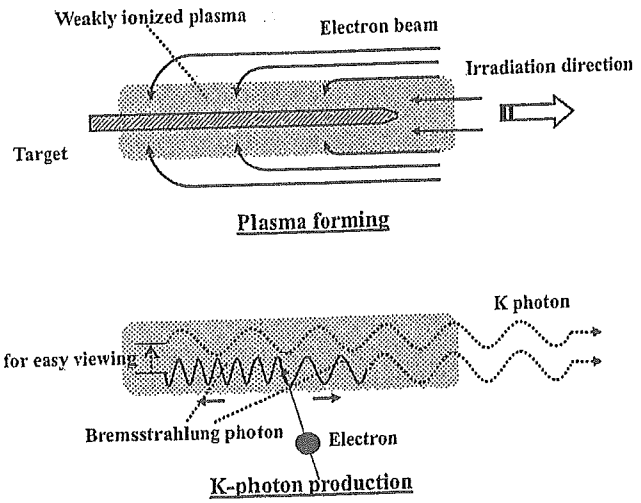

Fig. 4 K-photon irradiation from weakly ionized plasma.

sequently, Kβ rays (8.90 keV) are absorbed effectively using a 10-μm-thick nickel K-edge filter with an edge of 8.33 keV, and quite clean Kα rays (8.04 keV) are produced.

3 Characteristics

3.1 *Tube Voltage and Current*

Tube voltage and current were measured by a high-voltage divider with an input impedance of 1 GΩ and a current transformer, respectively. Figure 5 shows the time relation for the tube voltage and current. At the indicated charging voltages, they roughly displayed damped oscillations. When the charging voltage was increased, both the maximum tube voltage and current increased. At a charging voltage of 50 kV, the maximum tube voltage was almost equal to the charging voltage of the main condenser, and the maximum tube current was approximately 15 kA.

3.2 *X-Ray Output*

An x-ray output pulse was detected using a combination of a plastic scintillator and a photomultiplier using a 10-μm-thick monochromatic copper filter (Fig. 6). The x-ray pulse height substantially increased with corresponding increases in the charging voltage. The x-ray pulse widths were about 700 ns, and the time-integrated x-ray intensity per pulse measured by a thermoluminescence dosimeter (Kyokko TLD Reader 1500 utilizing MSO-S elements without energy compensation) had a value of about 20 μC/kg at 1.0 m from the x-ray source, with a charging voltage of 50 kV.

3.3 *X-Ray Source*

To measure images of the Kα source, we employed a pinhole camera with a hole diameter of 100 μm (Fig. 7). When the charging voltage was increased, the plasma x-ray source grew, and both spot dimension and intensity increased. Because the x-ray intensity is the highest at the center of the spot, both the dimension and intensity decreased according to both increases in the thickness of a filter for absorbing x-rays and decreases in the pinhole diameter.

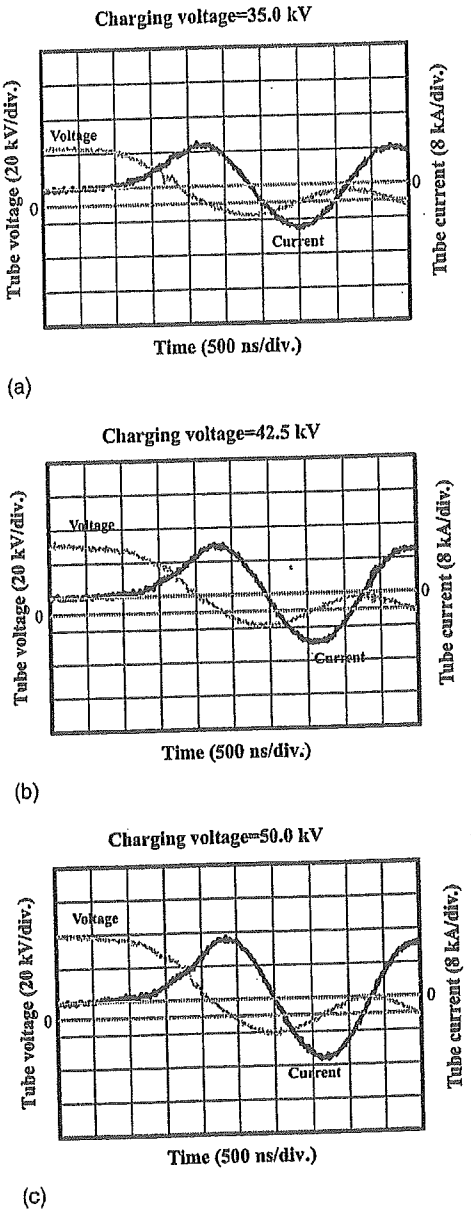

Fig. 5 Tube voltages and currents with charging voltage of (a) 35.0 kV, (b) 42.5 kV, and (c) 50.0 kV.

3.4 *X-Ray Spectra*

X-ray spectra from the plasma source were measured using a transmission-type spectrometer with a lithium fluoride

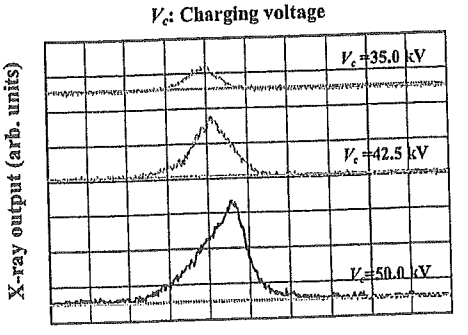

Fig. 6 X-ray outputs measured by plastic scintillator with changes in charging voltage.

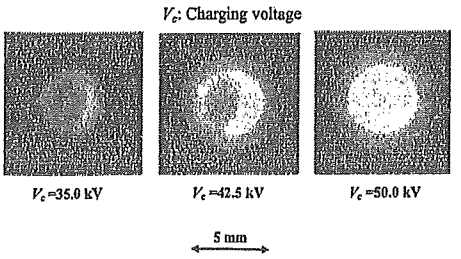

Fig. 7 Images of Kα x-ray source measured by pinhole of 100 μm from plasma axial direction.

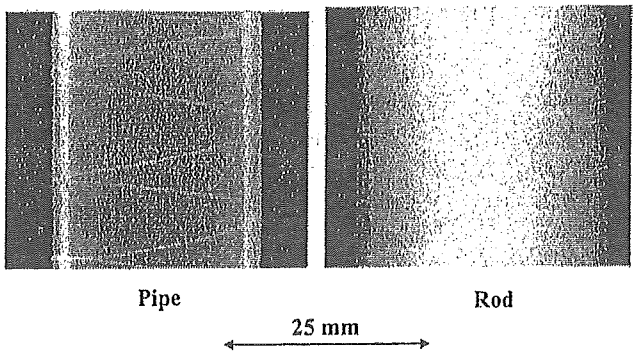

Fig. 9 Radiograms of tungsten wires 50 μm in diameter coiled around pipe, and rod made of polymethyl methacrylate.

curved crystal 0.5 mm in thickness. The spectra were taken by a computed radiography (CR) system[21] (Konica Regius 150) with a wide dynamic range, using the filter, and relative x-ray intensity was calculated from Dicom digital data. Figure 8 shows measured spectra from the copper target using the filter. In fact, we observed clean Kα lines such as lasers, and confirmed the significant filtering effect, while bremsstrahlung rays were hardly detected at all. The characteristic x-ray intensity of the Kα lines substantially increased with corresponding increases in the charging voltage, and the Kβ line was absorbed by the filter. Although this spectrometer has sufficient energy resolution for measuring Kα_1 and Kα_2 lines, we could observe only a single line.

4 Radiography

Plasma radiography was performed by the CR system without using the filter, and the distance between the x-ray source and imaging plate was 1.2 m.

First, rough measurements of image resolution were made using wires. Figure 9 shows radiograms of 50-μm-diam tungsten wires coiled around a pipe, and a rod made of polymethyl methacrylate with a charging voltage of 50 kV. Although the image contrast increased using the pipe, 50-μm-diam wires could be observed.

The image of water falling into a polypropylene beaker from a glass test tube is shown in Fig. 10. This image was taken with a charging voltage of 45 kV, with the slight addition of an iodine-based contrast medium. Because the x-ray duration was about 1 μs, the stop-motion image of water could be obtained.

Figure 11 shows an angiogram of a rabbit heart; iodine-based microspheres of 15 μm in diameter were used with a charging voltage of 50 kV, and fine blood vessels of about 100 μm were visible.

5 Discussion

Concerning the spectrum measurement, we obtained fairly clean Kα lines from a weakly ionized linear plasma x-ray

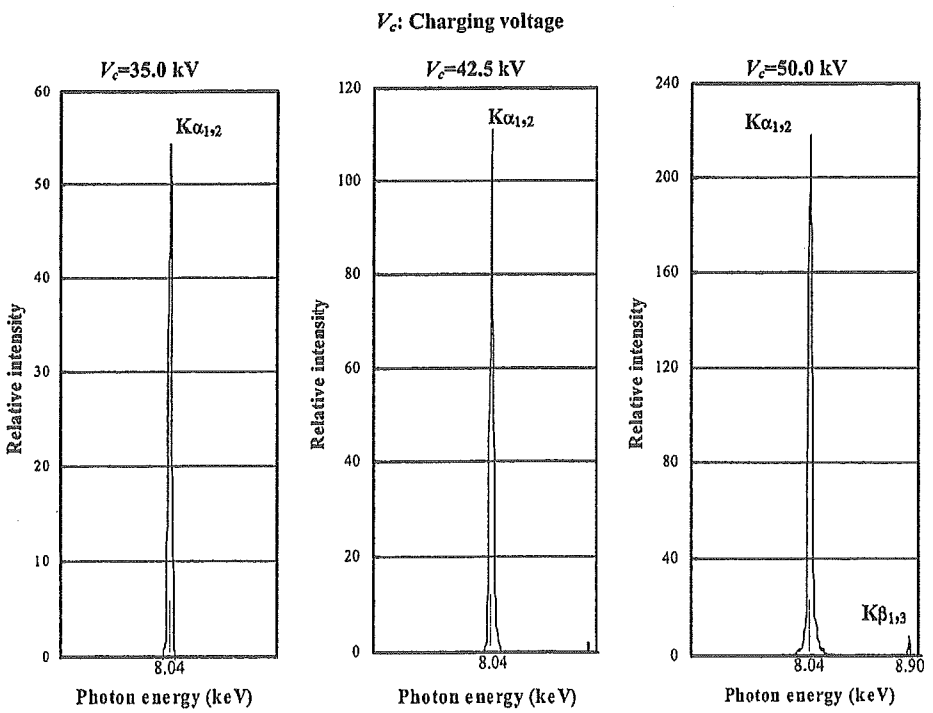

Fig. 8 X-ray spectra from weakly ionized copper plasma according to changes in charging voltage and to insertion of nickel K-edge filter.